

## Article

# Griffinite, $\text{Al}_2\text{TiO}_5$ : A New Oxide Mineral from Inclusions in Corundum Xenocrysts from the Mount Carmel Area, Israel

Chi Ma <sup>1,\*</sup>, Fernando Cámara <sup>2</sup>, Vered Toledo <sup>3</sup> and Luca Bindi <sup>4,\*</sup><sup>1</sup> Division of Geological and Planetary Sciences, California Institute of Technology, Pasadena, CA 91125, USA<sup>2</sup> Dipartimento di Scienze Della Terra “A. Desio”, Università Degli Studi di Milano, Via Mangiagalli 34, I-20133 Milan, Italy; fernando.camara@unimi.it<sup>3</sup> Shefa Gems (A.T.M.) Ltd., Netanya 4210602, Israel; veredshefa@gmail.com<sup>4</sup> Dipartimento di Scienze Della Terra, Università Degli Studi di Firenze, Via La Pira 4, I-50121 Florence, Italy

\* Correspondence: chima@caltech.edu (C.M.); luca.bindi@unifi.it (L.B.)

**Abstract:** Griffinite (IMA 2021-110), ideally  $\text{Al}_2\text{TiO}_5$ , is a new mineral from inclusions in corundum xenocrysts from the Mount Carmel area, Israel. It occurs as subhedral crystals,  $\sim 1\text{--}4 \mu\text{m}$  in size, together with Zr-rich rutile within a corundum grain. In this study, a mean of eight electron probe microanalyses gave  $\text{TiO}_2$  44.41 (24),  $\text{Al}_2\text{O}_3$  55.13 (18),  $\text{FeO}$  0.47 (5), and  $\text{MgO}$  0.37 (2), totaling 100.38 wt%, which corresponded, on the basis of a total of five oxygen atoms, to  $(\text{Al}_{1.97}\text{Mg}_{0.02}\text{Fe}_{0.01})\text{Ti}_{1.01}\text{O}_5$ . Electron back-scatter diffraction studies revealed that griffinite is orthorhombic and in the space group  $Cmcm$ , with  $a = 3.58$  (2) Å,  $b = 9.44$  (1) Å,  $c = 9.65$  (1) Å, and  $V = 326$  (2) Å<sup>3</sup> with  $Z = 4$ . The six strongest calculated powder diffraction lines [ $d$  in Å ( $I/I_0$ ) ( $hkl$ )] are 3.347 (100) (110); 2.658 (90) (023); 4.720 (77) (020); 1.903 (57) (043); 1.790 (55) (200); and 1.688 (44) (134). In the crystal structure,  $\text{Al}^{3+}$  and  $\text{Ti}^{4+}$  are disordered into two distinct distorted octahedra, which form edge-sharing double chains. Griffinite is a high-temperature oxide mineral, formed in melt pockets in corundum-aggregate xenoliths derived from the upper mantle beneath Mount Carmel, Israel. The new mineral is named after William L. Griffin, a geologist at Macquarie University, Australia.



**Citation:** Ma, C.; Cámara, F.; Toledo, V.; Bindi, L. Griffinite,  $\text{Al}_2\text{TiO}_5$ : A New Oxide Mineral from Inclusions in Corundum Xenocrysts from the Mount Carmel Area, Israel. *Crystals* **2023**, *13*, 1427. <https://doi.org/10.3390/crust13101427>

Academic Editors: Bo Xu and Ying Guo

Received: 11 September 2023

Revised: 22 September 2023

Accepted: 25 September 2023

Published: 26 September 2023



**Copyright:** © 2023 by the authors. Licensee MDPI, Basel, Switzerland. This article is an open access article distributed under the terms and conditions of the Creative Commons Attribution (CC BY) license (<https://creativecommons.org/licenses/by/4.0/>).

## 1. Introduction

Small Cretaceous volcanoes exposed on Mount Carmel (Northern Israel) and associated Plio-Pleistocene paleoplacers in the adjacent Kishon Valley contain xenoliths (up to cm size) comprising aggregates of corundum crystals with intercrystalline to interstitial melt pockets. The melt pockets and individual mineral inclusions in corundum contain a remarkable assemblage of minerals crystallized under highly reducing conditions [1].

During a study of melt inclusions in the corundum xenocrysts, we have identified seven IMA-approved new minerals since 2021: griffinite ( $\text{Al}_2\text{TiO}_5$ ), magnéliite ( $\text{Ti}^{3+}_2\text{Ti}^{4+}_2\text{O}_7$ ), ziroite ( $\text{ZrO}_2$ ), sassite ( $\text{Ti}^{3+}_2\text{Ti}^{4+}\text{O}_5$ ), mizraite-(Ce) ( $\text{Ce}(\text{Al}_{11}\text{Mg})\text{O}_{19}$ ), toledoite ( $\text{TiFeSi}$ ), and yeite ( $\text{TiSi}$ ) [2–8]. Reported here is the new mineral griffinite, the first natural occurrence of  $\text{Al}_2\text{TiO}_5$  in a corundum xenocryst from Mount Carmel (Figure 1), providing more insights into the origin of high-temperature minerals from the upper mantle.

The new oxide mineral has been named in honor of William L. Griffin (b. 1941), a geologist at Macquarie University, Australia, for his outstanding contributions to mineralogy, petrology, and geochemistry of the deep crust and lithospheric mantle, including intense investigations of materials from the Mount Carmel area. Griffinite was approved as a new mineral by the IMA-CNMNC (2021-110) [2]. Noteworthily, synthetic ceramic  $\text{Al}_2\text{TiO}_5$  is known in the scientific literature as an excellent thermal-shock-resistant material referred to as *tialite* and *tielite* (e.g., [9,10]).  $\text{Al}_2\text{TiO}_5$  has a very low thermal expansion ( $1.5 \times 10^{-6} \text{ K}^{-1}$ ), low Young’s modulus, and high-temperature resistance (melting point  $1860 \pm 10^\circ\text{C}$ ; [11]).

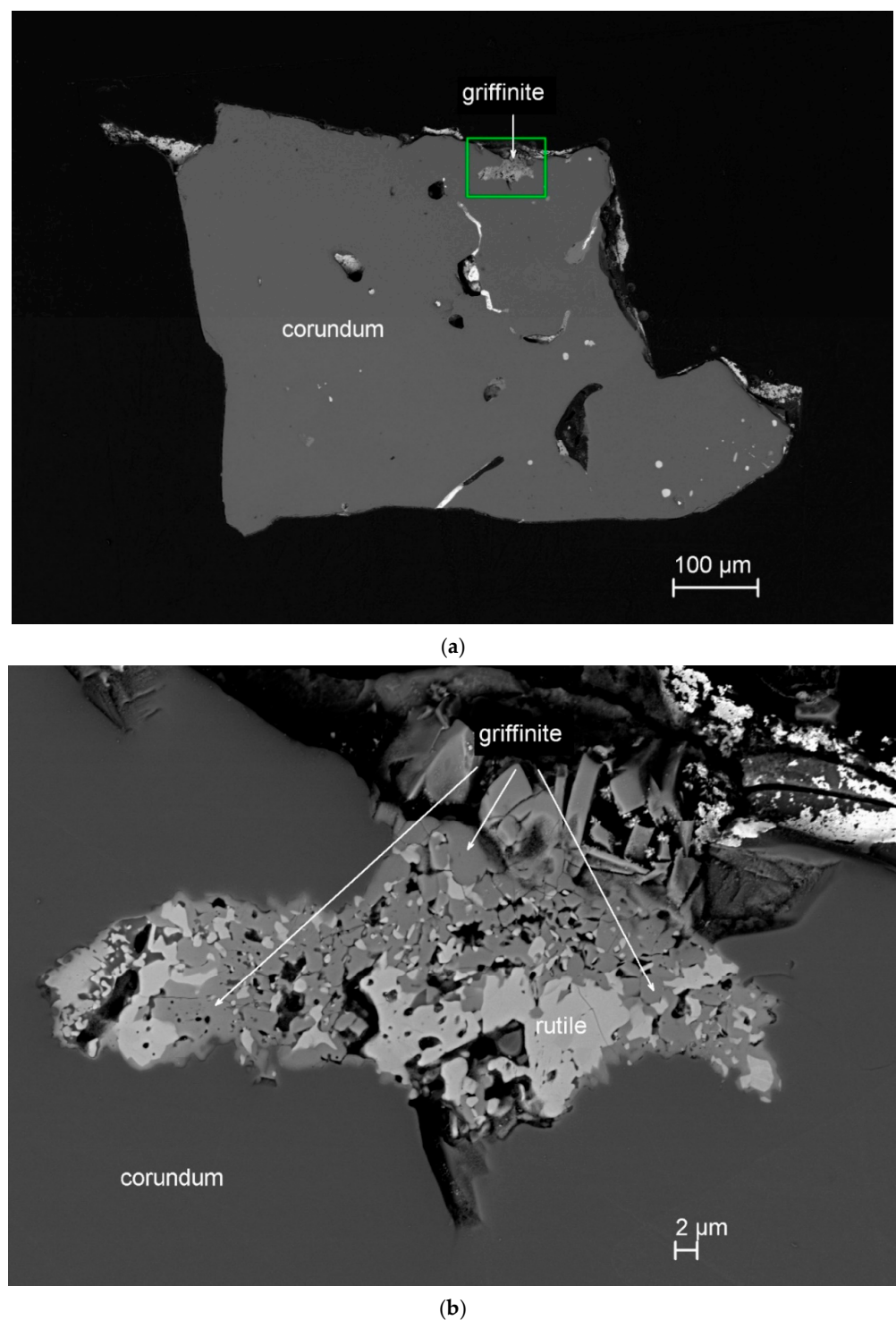


**Figure 1.** SEM back-scatter electron images showing type griffinite ( $\text{Al}_2\text{TiO}_5$ ). (a) Griffinite in corundum grain 198c from Mount Carmel mount Corundum-18-1. (b) A close-up of griffinite with rutile. The green rectangle in panel (a) indicates the region enlarged in panel (b).

## 2. Materials and Methods

The corundum xenolith in which we found the type griffinite occurs in a Plio-Pleistocene placer gemstone deposit in the Kishon River, which drains Mount Carmel and the adjacent Yizre’el Valley and enters the sea near Haifa in Northern Israel [12]. It is part of a xenolith assemblage that includes aggregates of skeletal corundum crystals with melt pockets containing reduced mineral assemblages [12–16].

The material used in the present study came from both volcanic centers on Mount Carmel, N. Israel, and alluvial deposits derived from these and Miocene to Pliocene basalts exposed in the Yisre’el Valley. The holotype material in one corundum grain (No. 198c) from Mount Carmel mount Corundum-18-1 is deposited in the mineralogy collection of the Università degli Studi di Milano, Via Mangiagalli, 34—20133 Milano, Italy, registration number MCMGPG-H2022-002.

A ZEISS 1550VP Field-Emission Scanning Electron Microscope (SEM) (ZEISS Group, Jena, Germany) with an Oxford X-Max energy-dispersive spectroscopy (EDS) (Oxford Instruments, Abingdon, UK) device was used for backscatter electron (BSE) imaging and fast elemental analysis. A preliminary chemical analysis using EDS performed on the crystal fragment used for the structural study did not indicate the presence of elements ( $Z > 9$ ) other than Ti, Al, O, and minor Fe and Mg. Electron probe microanalyses (EPMA) were carried out using a JEOL 8200 Superprobe (JEOL Ltd., Tokyo, Japan) (WDS mode, 15 kV, 10 nA, focused beam = ~150 nm in diameter) on griffinit crystals in polished corundum grain 198c with a 25 nm carbon coating, as shown in Figure 1. The following lines were used: Ti  $K\alpha$ , Al  $K\alpha$ , Mg  $K\alpha$ , and Fe  $K\alpha$ . The standards employed were synthetic  $TiO_2$  (Ti), anorthite (Al), fayalite (Fe), and forsterite (Mg). Quantitative elemental microanalyses were processed with the CITZAF correction procedure [17]. The crystal fragment was found to be homogeneous within analytical error. The analytical results of griffinit are given in Table 1.

**Table 1.** Electron microprobe analysis (wt% of oxides) of griffinit.

Constituent (wt%)	Mean (n = 8)	Range	SD	Probe Standard
$TiO_2$	44.41	44.15–44.71	0.24	$TiO_2$
$Al_2O_3$	55.13	54.90–55.34	0.18	anorthite
FeO	0.47	0.40–0.58	0.05	fayalite
MgO	0.37	0.36–0.40	0.02	forsterite
Total	100.38			

Conventional X-ray studies could not be carried out because of the small crystal size. Electron backscatter diffraction (EBSD) analyses were performed using the methods described in [18,19] for micron-sized new mineral studies. An HKL EBSD system on a ZEISS 1550VP Field-Emission SEM was operated at 20 kV and 6 nA in focused beam mode with a 70°-tilted stage and in a variable pressure mode (25 Pa) on griffinit crystals in polished corundum grain 198c without any coating. The focused electron beam was several nanometers in diameter. The spatial resolution for diffracted backscatter electrons was ~30 nm in size [20]. The EBSD system was calibrated using a single-crystal silicon standard. Structural information and cell constants were obtained by matching the experimental EBSD patterns with structures of Al-Ti-O and Ti-O phases from the ICSD [21,22].

### 3. Results

Griffinit in the type material occurs as subhedral crystals, ~1–4  $\mu m$  in size, together with Zr-rich rutile within corundum grain 198c in the polished 1-inch mount Corundum-18-1 (Figure 1). This association forms pseudomorphs and appears to reflect the oxidation breakdown of carmeltazite ( $ZrAl_2Ti_4O_{11}$ ). Other inclusions in this corundum grain contain yeite (TiSi), baddeleyite, hibonite, osbornite (TiN), khamrabaevite (TiC), Ti,Al,Zr-oxide, and zirconolite. Griffinit is transparent and, given the size, most of the physical and optical properties could not be obtained. Griffinit has also been observed to crystallize directly from melts trapped between corundum grains.

The average chemical compositions (eight analyses of different spots on four larger crystals in the same inclusion in Figure 1) together with the wt% ranges of elements are reported in Table 1. Fe and Ti were considered di- and tetravalent, respectively. On the basis of five oxygen atoms, the empirical formula of griffinit is  $(Al_{1.97}Mg_{0.02}Fe_{0.01})Ti_{1.01}O_5$ .

The simplified ideal formula is  $(\text{Al},\text{Mg},\text{Fe},\text{Ti})_2\text{TiO}_5$ , and the ideal formula is  $\text{Al}_2\text{TiO}_5$  ( $Z = 4$ ), which requires  $\text{Al}_2\text{O}_3$  56.07 and  $\text{TiO}_2$  43.93, totaling 100 wt%.

The EBSD patterns of griffinite can be indexed only by the *Cmcm* pseudobrookite-type structure and match to the cell values reported for synthetic  $\text{Al}_2\text{TiO}_5$  cells by [21,22] (Figure 2), with a mean angular deviation of  $0.32^\circ$ – $0.38^\circ$ , revealing the following cell parameters:  $a = 3.58(2)$  Å,  $b = 9.44(1)$  Å,  $c = 9.65(1)$  Å, and  $V = 326(2)$  Å<sup>3</sup> with  $Z = 4$ .

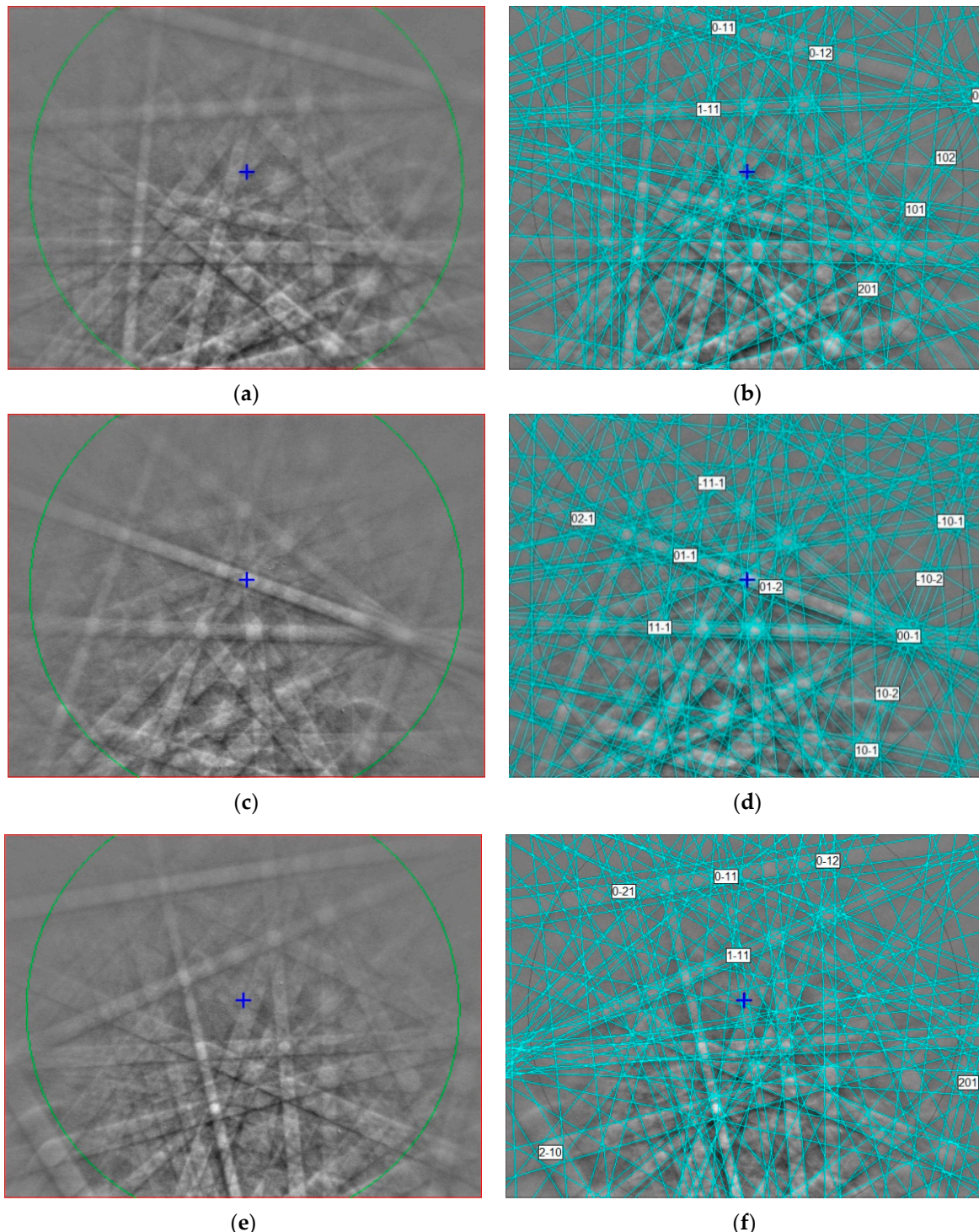


**Figure 2.** (a,c,e) EBSD patterns of three griffinite crystals in Figure 1 at different orientations, and (b,d,f) the patterns indexed with the *Cmcm*  $\text{Al}_2\text{TiO}_5$  pseudobrookite-type structure. The blue cross shows pattern center; the blue lines are calculated diffraction bands.

X-ray powder diffraction data (Table 2, in Å for CuK $\alpha$ , Bragg–Brentano geometry) were calculated with the unit cell parameters above, the crystallographic data of synthetic Al<sub>2</sub>TiO<sub>5</sub> [23], and the empirical formula, using Powder Cell version 2.4.

**Table 2.** Calculated X-ray powder diffraction data for griffinite ( $I_{\text{rel}} > 1$ ). Reflections with  $I_{\text{rel}} > 25\%$  are evidenced in bold.

<i>h</i>	<i>k</i>	<i>l</i>	<i>d</i> (Å)	<i>I</i> <sub>rel</sub>
0	0	2	4.825	1
<b>0</b>	<b>2</b>	<b>0</b>	<b>4.720</b>	<b>77</b>
0	2	1	4.240	2
0	2	2	3.374	24
<b>1</b>	<b>1</b>	<b>0</b>	<b>3.347</b>	<b>100</b>
<b>1</b>	<b>1</b>	<b>1</b>	<b>3.163</b>	<b>39</b>
<b>0</b>	<b>2</b>	<b>3</b>	<b>2.658</b>	<b>90</b>
0	0	4	2.413	1
1	3	0	2.364	13
0	4	0	2.360	1
1	1	3	2.319	15
<b>0</b>	<b>2</b>	<b>4</b>	<b>2.148</b>	<b>26</b>
1	3	2	2.123	6
0	4	2	2.120	17
<b>0</b>	<b>4</b>	<b>3</b>	<b>1.903</b>	<b>57</b>
<b>2</b>	<b>0</b>	<b>0</b>	<b>1.790</b>	<b>55</b>
0	2	5	1.786	5
<b>1</b>	<b>3</b>	<b>4</b>	<b>1.688</b>	<b>44</b>
2	2	0	1.674	9
1	1	5	1.672	1
1	5	0	1.670	2
0	0	6	1.608	21
2	2	2	1.581	5
1	5	2	1.578	19
0	6	0	1.573	8
0	6	1	1.553	7
0	2	6	1.522	10
0	6	2	1.496	1
1	3	5	1.495	7
0	4	5	1.494	1
<b>2</b>	<b>2</b>	<b>3</b>	<b>1.485</b>	<b>32</b>
<b>1</b>	<b>5</b>	<b>3</b>	<b>1.482</b>	<b>26</b>
1	1	6	1.450	4
2	0	4	1.438	1
2	4	0	1.426	1
2	2	4	1.375	11
1	5	4	1.373	8
2	4	2	1.368	8
1	3	6	1.330	7
0	2	7	1.323	4
<b>2</b>	<b>4</b>	<b>3</b>	<b>1.304</b>	<b>30</b>
1	1	7	1.275	13
2	2	5	1.265	3
1	7	0	1.262	1
1	7	1	1.251	14
1	7	2	1.221	10
0	6	5	1.220	3
2	0	6	1.196	14
3	1	0	1.184	4
2	6	0	1.182	6

#### 4. Discussion

Griphinite is a new member of the pseudobrookite group. Griphinite ( $\text{Al}_2\text{TiO}_5$ ) is the second Al-Ti-oxide mineral, joining machiite ( $\text{Al}_2\text{Ti}_3\text{O}_9$ ) [24]. Both are high-temperature minerals. Machiite is an ultrarefractory phase from the solar nebula. There is also a chance that griphinite might occur as a refractory phase in the solar nebula.

By analogy with synthetic  $\text{Al}_2\text{TiO}_5$ , griphinite is isostructural with pseudobrookite ( $\text{Fe}^{3+}_2\text{TiO}_5$ ), armalcolite ( $(\text{Fe}^{2+}, \text{Mg})\text{Ti}_2\text{O}_5$ ), and sassite ( $(\text{Ti}^{3+}_2\text{Ti}^{4+}\text{O}_5)$  [5]). In the synthetic  $\text{Al}_2\text{TiO}_5$  structure,  $\text{Al}^{3+}$  and  $\text{Ti}^{4+}$  are disordered into two distinct distorted octahedra (Wyckoff positions  $4c$  and  $8f$ ). Such  $(\text{Al}, \text{Ti})\text{O}_6$  octahedra form edge-sharing double chains [21,22]. The crystal structure is shown in Figure 3. Studies on synthetic  $\text{Al}_2\text{TiO}_5$  indicate that griphinite may show significant cation disorder among octahedra [23,25]. Synthetic  $\text{Al}_2\text{TiO}_5$  is thermodynamically stable at  $T > 1280^\circ\text{C}$  [26]. At lower temperatures, it decomposes to corundum + rutile. The formation temperature of synthetic  $\text{Al}_2\text{TiO}_5$  is lowered to  $<1280^\circ\text{C}$  in the presence of Mg [27,28] and low diffusion. However, the instability temperature range is restricted to  $T > 1100^\circ\text{C}$  [29]. The process of decomposition of synthetic  $\text{Al}_2\text{TiO}_5$  is also strongly affected by the oxygen partial pressure [29].

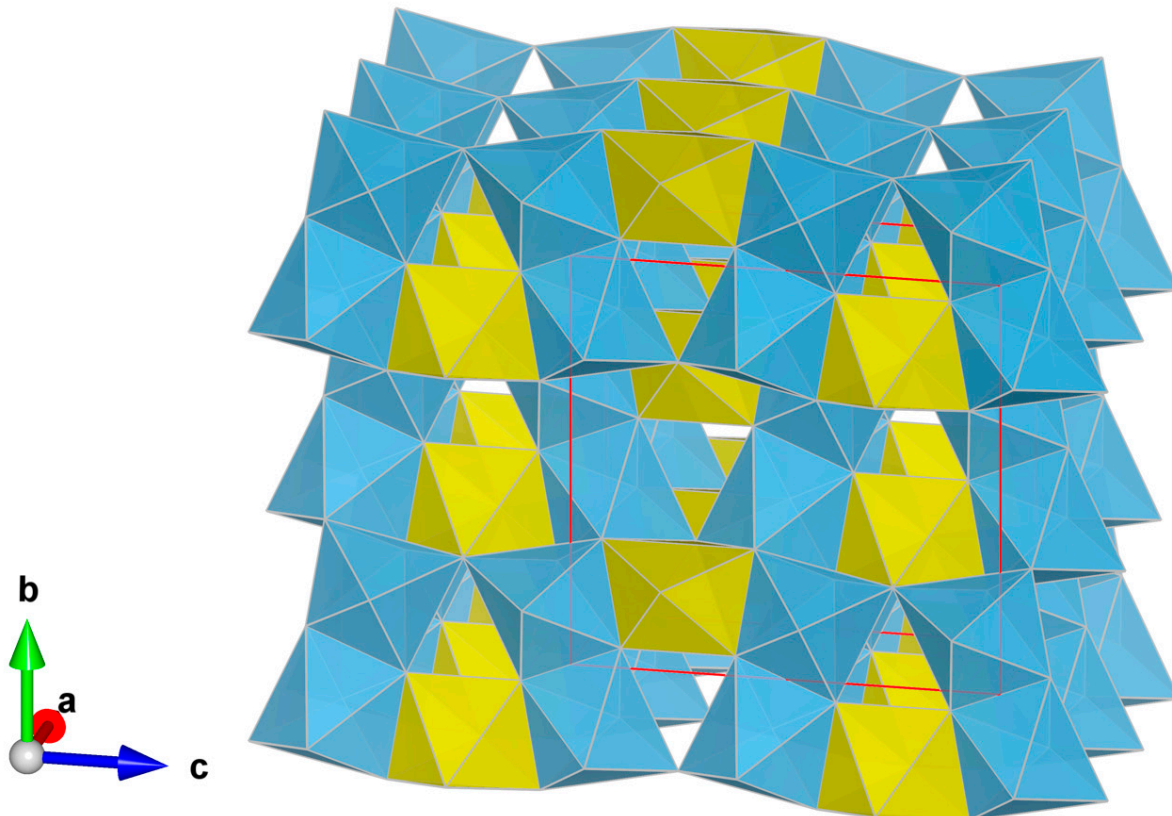


**Figure 3.** The crystal structure of griphinite down [100] (perspective view).  $(\text{Al}, \text{Ti})\text{O}_6$  octahedra are depicted in yellow (Wyckoff  $4c$ ) and light blue (Wyckoff  $8f$ ), respectively. The unit cell (red) and the orientation of the structure are shown. Figure obtained with Vesta 3.0 [30].

Upon heating, synthetic  $\text{Al}_2\text{TiO}_5$  tends to contract in the direction of its stronger bonding apex-sharing oxygens, i.e., the  $a$ -axis, meaning negative thermal expansion in this direction [23] showing  $\alpha_a = -2.38(32) \times 10^{-6}\text{ K}^{-1}$  [22].

Griphinite is a high-temperature ( $>1300$ –ca.  $1150^\circ\text{C}$ ) phase crystallized from melts trapped in voids of corundum crystals [12,31]. The mineralogical assemblage demonstrates an oxygen fugacity ( $f\text{O}_2$ ) below the levels usually observed in Earth's crust or upper mantle (IW to IW-9; [32]). The extreme reduction observed requires a hydrogen-dominated environment, as proved by the presence of natural hydrides and hydrogen in vacancies

in hibonite [14,32–34], and reflects the reduction and desilication of differentiated syenitic melts, through interaction with mantle-derived  $\text{CH}_4 + \text{H}_2$  fluids [32,35,36]. The desilication of the melts as well as the separation of  $\text{Si}^0$  melts and Fe-Ti-Si melts drive the supersaturation of  $\text{Al}_2\text{O}_3$  in the silicate melts and lead to the crystallization of large corundum crystals. Other minerals present in the melt inclusions in corundum xenocrysts from the Mount Carmel area are reported in Figure 4.

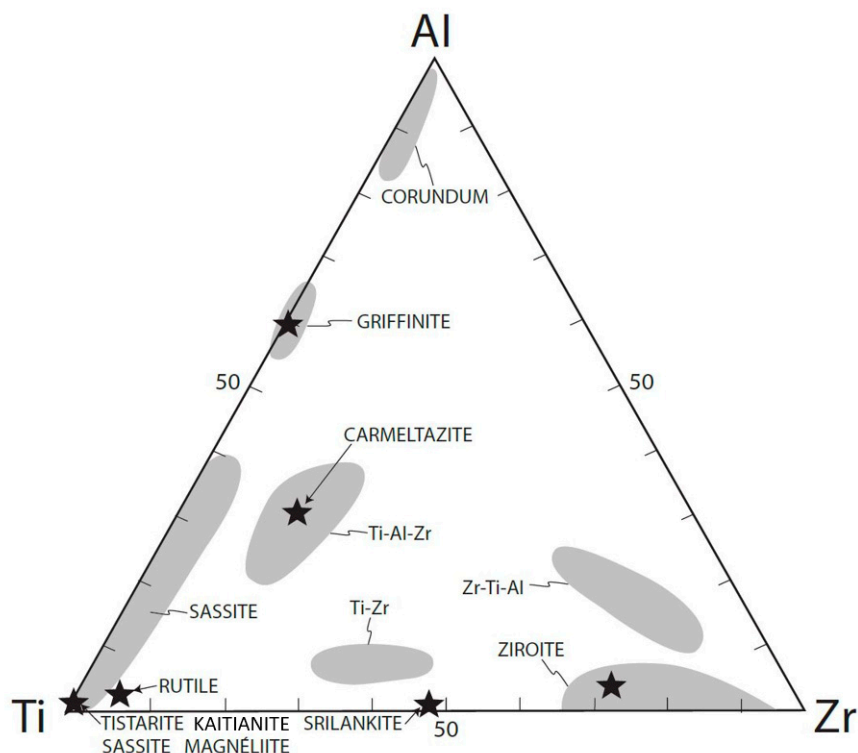


**Figure 4.** Ti-Al-Zr triplot showing phases with various compositions from melt inclusions in corundum xenocrysts from the Mount Carmel area, from [37].

Among the corundum aggregates, three types of paragenesis can be recognized [31].

Crn-A: Strongly Ti-zoned hopper crystals [36]. The trapped melts are Ca-Mg-Al silicates with high sulfur content and incompatible elements. The phase assemblages ( $\text{Ti}^{3+}$  in oxides and  $\text{Ti}^{2+}$  in carbides and borides) reflect  $f\text{O}_2 \leq \text{IW-6}$ .

Crn-B: Large Ti-poor corundum crystals, with trapped pockets exhibiting small amounts of Ca-Al-Mg silicate glass, typically high in REE, Zr, Th, U, and other incompatible elements. Ti is present as both  $\text{Ti}^{3+}$  and  $\text{Ti}^{4+}$ .

Crn-C: Similar to Crn-B but with lower Ti contents. Rare Ca-Al-Na-K silicate glasses are rich in LREE and Ba. The presence of more abundant  $\text{Ti}^{4+}$  phases indicates a higher mean  $f\text{O}_2$  than in Crn-A and Crn-B.

The identification of the different valence states of the diverse phases in the three parageneses indicates that Crn-B and Crn-C are cumulates from immiscible Fe-rich melts (subsequently depleted in Fe by the separation of Fe-Ti silicide melts; [1]) and Si-Al-Na-K melts, respectively. It is likely that these melts have similar but divergent histories, separated into volumes that were affected to different extents by interaction with the reducing ( $\text{CH}_4 + \text{H}_2$ ) fluids before being entrained in the host basalt.

**Author Contributions:** Conceptualization, C.M., F.C. and L.B.; methodology, C.M.; formal analysis, C.M., F.C. and L.B.; investigation, C.M., F.C. and L.B.; resources, V.T.; data curation, C.M.; writing—original draft, C.M.; writing—review and editing, C.M., F.C. and L.B. All authors have read and agreed to the published version of the manuscript.

**Funding:** The research was funded by MIUR-PRIN2017, project “TEOREM deciphering geological processes using Terrestrial and Extraterrestrial ORE Minerals”, prot. 2017AK8C32 (PI: Luca Bindi).

**Data Availability Statement:** Data are available from C.M.

**Acknowledgments:** We sincerely thank William L. Griffin for the detailed discussion on the background information and origin of this new mineral. We thank three reviewers for their constructive reviews. SEM, EBSD, and EPMA analyses were carried out at the Caltech GPS Division Analytical Facility, which is supported, in part, by NSF Grants EAR-0318518 and DMR-0080065.

**Conflicts of Interest:** The authors declare no conflict of interest.

## References

1. Griffin, W.L.; Gain, S.E.M.; Saunders, M.; Huang, J.-X.; Alard, O.; Toledo, V.; O'Reilly, S.Y. Immiscible metallic melts in the upper mantle beneath Mount Carmel, Israel: Silicides, phosphides and carbides. *Am. Mineral.* **2022**, *107*, 532–549. [[CrossRef](#)]
2. Ma, C.; Bindi, L.; Cámara, F.; Toledo, V. Griffinite, IMA 2021-110, in: CNMNC Newsletter 66. *Eur. J. Mineral.* **2022**, *34*, 253–257.
3. Ma, C.; Griffin, W.L.; Bindi, L.; Cámara, F.; Toledo, V. Magnéliite, IMA 2021-111, in CNMNC Newsletter 66. *Miner. Mag.* **2022**, *86*, 362.
4. Ma, C.; Griffin, W.L.; Bindi, L.; Cámara, F.; Toledo, V. Ziroite, IMA 2022-013, in CNMNC Newsletter 68. *Miner. Mag.* **2022**, *86*, 854–855.
5. Ma, C.; Griffin, W.L.; Bindi, L.; Cámara, F.; Toledo, V. Sassite, IMA 2022-014, in CNMNC Newsletter 68. *Miner. Mag.* **2022**, *86*, 855.
6. Ma, C.; Griffin, W.L.; Bindi, L.; Cámara, F.; Toledo, V. Mizraite-(Ce), IMA 2022-027, in CNMNC Newsletter 68. *Miner. Mag.* **2022**, *86*, 857.
7. Ma, C.; Griffin, W.L.; Bindi, L.; Cámara, F. Toledoite, IMA 2022-036, in CNMNC Newsletter 66. *Miner. Mag.* **2022**, *86*, 858.
8. Ma, C.; Griffin, W.L.; Bindi, L.; Cámara, F.; Toledo, V. Yeite, IMA 2022-079, in CNMNC Newsletter 70. *Miner. Mag.* **2022**, *87*, 165.
9. Yamaguchi, G. Studies on tialilite  $\text{Al}_2\text{O}_3\text{-TiO}_2$ . *J. Ceram. Soc. Jpn.* **1944**, *52*, 6–7.
10. Kalpaki, Y. Effect of  $\text{TiO}_2$  addition on  $\text{Al}_2\text{TiO}_5$  (tialilite) phase evolution of *in situ*  $\text{MgAl}_2\text{O}_4$  formation zero cement castable (ZCC). *Adv. Appl. Ceram.* **2014**, *113*, 282–289. [[CrossRef](#)]
11. Huang, Y.X.; Senos, A.M.R.; Baptista, J.L. Thermal and mechanical properties of aluminium titanate–mullite composites. *J. Mater. Res.* **2000**, *15*, 357–363. [[CrossRef](#)]
12. Griffin, W.L.; Gain, S.E.M.; Bindi, L.; Toledo, V.; Cámara, F.; Saunders, M.; O'Reilly, S.Y. Carmeltazite,  $\text{ZrAl}_2\text{Ti}_4\text{O}_{11}$ , a new mineral trapped in corundum from volcanic rocks of Mt Carmel, northern Israel. *Minerals* **2018**, *8*, 601–612. [[CrossRef](#)]
13. Griffin, W.L.; Gain, S.E.M.; Adams, D.T.; Huang, J.-X.; Saunders, M.; Toledo, V.; Pearson, N.J.; O'Reilly, S.Y. First terrestrial occurrence of tistarite ( $\text{Ti}_2\text{O}_3$ ): Ultra-low oxygen fugacity in the upper mantle beneath Mt Carmel, Israel. *Geology* **2016**, *44*, 815–818. [[CrossRef](#)]
14. Griffin, W.L.; Gain, S.E.M.; Huang, J.-X.; Saunders, M.; Shaw, J.; Toledo, V.; O'Reilly, S.Y. A terrestrial magmatic hibonite–grossite–vanadium assemblage: Desilication and extreme reduction in a volcanic plumbing system, Mt Carmel, Israel. *Am. Mineral.* **2019**, *104*, 207–217. [[CrossRef](#)]
15. Griffin, W.L.; Toledo, V.; O'Reilly, S.Y. Discussion of “Enigmatic super-reduced phases in corundum from natural rocks: Possible contamination from artificial abrasive materials or metallurgical slags” by Litasov et al. *Lithos* **2019**, *348–349*, 105122. [[CrossRef](#)]
16. Xiong, Q.; Griffin, W.L.; Huang, J.-X.; Gain, S.E.M.; Toledo, V.; Pearson, N.J.; O'Reilly, S.Y. Super-reduced mineral assemblages in “ophiolitic” chromitites and peridotites: The view from Mt. Carmel. *Eur. J. Mineral.* **2017**, *29*, 557–570. [[CrossRef](#)]
17. Armstrong, J.T. CITZAF: A package of correction programs for the quantitative electron microbeam X-ray analysis of thick polished materials, thin films, and particles. *Microbeam Anal.* **1995**, *4*, 177–200.
18. Ma, C.; Rossman, G.R. Barioperovskite,  $\text{BaTiO}_3$ , a new mineral from the Benitoite Mine, California. *Am. Mineral.* **2008**, *93*, 154–157. [[CrossRef](#)]
19. Ma, C.; Rossman, G.R. Tistarite,  $\text{Ti}_2\text{O}_3$ , a new refractory mineral from the Allende meteorite. *Am. Mineral.* **2009**, *94*, 841–844. [[CrossRef](#)]
20. Chen, D.; Kuo, J.-C.; Wu, W.-T. Effect of microscopic parameters on EBSD spatial resolution. *Ultramicroscopy* **2011**, *111*, 1488–1494. [[CrossRef](#)]
21. Austin, A.E.; Schwartz, C.M. The crystal structure of aluminium titanate. *Acta Crystallogr.* **1953**, *6*, 812–813. [[CrossRef](#)]
22. Skala, R.D.; Li, D.; Low, I.M. Diffraction, structure and phase stability studies on aluminium titanate. *J. Eur. Ceram. Soc.* **2009**, *29*, 67–75. [[CrossRef](#)]
23. Morosin, B.; Lynch, R.W. Structure studies on  $\text{Al}_2\text{TiO}_5$  at room temperature and at 600 °C. *Acta Crystallogr.* **1972**, *B28*, 1040–1046. [[CrossRef](#)]
24. Krot, A.N.; Nagashima, K.; Rossman, G.R. Machiite,  $\text{Al}_2\text{Ti}_3\text{O}_9$ , a new oxide mineral from the Murchison carbonaceous chondrite: A new ultra-refractory phase from the solar nebula. *Am. Mineral.* **2020**, *105*, 239–243. [[CrossRef](#)]

25. Ohya, Y.; Kawauchi, Y.; Ban, T. Cation distribution of pseudobrookite-type titanates and their phase stability. *J. Ceram. Soc.* **2017**, *125*, 695–700. [[CrossRef](#)]
26. Kato, E.; Daimon, K.; Kobayashi, Y. Decomposition temperature of  $\beta$ -Al<sub>2</sub>TiO<sub>5</sub>. *J. Am. Ceram. Soc.* **1980**, *63*, 355–356. [[CrossRef](#)]
27. Lashkari, S.; Ebadi-Zadeh, T. Microwave sintering of Al<sub>2(1-x)</sub>Mg<sub>x</sub>Ti<sub>(1+x)</sub>O<sub>5</sub> ceramics obtained from mixture of nano-sized oxide powders. *Ceram. Int.* **2014**, *40*, 12669–12674. [[CrossRef](#)]
28. Basnet, B.; Sarkar, N.; Park, J.G.; Mazumder, S.; Kim, I.J. Al<sub>2</sub>O<sub>3</sub>–TiO<sub>2</sub>/ZrO<sub>2</sub>–SiO<sub>2</sub> based porous ceramics from particle-stabilized wet foam. *J. Adv. Ceram.* **2017**, *6*, 129–138. [[CrossRef](#)]
29. Low, I.M.; Oo, Z.; O’Connor, B.H. Effect of atmospheres on the thermal stability of aluminium titanate. *Phys. B Condens. Matter* **2006**, *385–386*, 502–504. [[CrossRef](#)]
30. Momma, K.; Izumi, F. VESTA 3 for three-dimensional visualization of crystal, volumetric and morphology data. *J. Appl. Crystallogr.* **2011**, *44*, 1272–1276. [[CrossRef](#)]
31. Griffin, W.L.; Bindi, L.; Cámarra, F.; Ma, C.; Gain, S.E.M.; Saunders, M.; Alard, O.; Huang, J.-X.; Shaw, J.; Meredith, C.; et al. Interactions of magmas and highly reduced fluids during intraplate volcanism, Mt Carmel, Israel: Implications for mantle redox states and global carbon cycles. *Gondwana Res.* **2023**; *in review*.
32. Griffin, W.L.; Gain, S.E.M.; Cámarra, F.; Bindi, L.; Shaw, J.; Alard, O.; Saunders, M.; Huang, J.-X.; Toledo, V.; O'Reilly, S.Y. Extreme reduction: Mantle-derived oxide xenoliths from a hydrogen-rich environment. *Lithos* **2020**, *358*, 105404. [[CrossRef](#)]
33. Bindi, L.; Cámarra, F.; Griffin, W.L.; Huang, J.-X.; Gain, S.E.M.; Toledo, V.; O'Reilly, S.Y. Discovery of the first natural hydride. *Am. Miner.* **2019**, *104*, 611–614. [[CrossRef](#)]
34. Bindi, L.; Cámarra, F.; Gain, S.E.M.; Griffin, W.L.; Huang, J.-X.; Saunders, M.; Toledo, V. Kishonite, VH<sub>2</sub>, and oreillyite, Cr<sub>2</sub>N, two new minerals from the corundum xenocrysts of Mt Carmel, Northern Israel. *Minerals* **2020**, *10*, 1118. [[CrossRef](#)]
35. Griffin, W.L.; Gain, S.E.M.; Saunders, M.; Cámarra, F.; Bindi, L.; Spartà, D.; Toledo, V.; O'Reilly, S.Y. Cr<sub>2</sub>O<sub>3</sub> in corundum: Ultra-high contents under reducing conditions. *Am. Mineral.* **2021**, *106*, 1420–1437. [[CrossRef](#)]
36. Oliveira, B.B.; Griffin, W.L.; Gain, S.E.M.; Saunders, M.; Shaw, J.; Toledo, V.; Afonso, J.C.; O'Reilly, S.Y. Ti<sup>3+</sup> in corundum: Tracing crystal growth in a highly reduced magma. *Sci. Rep.* **2021**, *11*, 2439. [[CrossRef](#)]
37. Ma, C.; Cámarra, F.; Bindi, L.; Toledo, V.; Griffin, W.L. First terrestrial occurrence of kaitianite (Ti<sup>3+</sup><sub>2</sub>Ti<sup>4+</sup>O<sub>5</sub>) from the Upper Mantle beneath Mount Carmel, Israel. *Minerals* **2023**, *13*, 1097. [[CrossRef](#)]

**Disclaimer/Publisher’s Note:** The statements, opinions and data contained in all publications are solely those of the individual author(s) and contributor(s) and not of MDPI and/or the editor(s). MDPI and/or the editor(s) disclaim responsibility for any injury to people or property resulting from any ideas, methods, instructions or products referred to in the content.